Olefin-linked covalent organic framework nanotubes based on triazine for selective oxidation of sulfides with O_2 powered by blue light

Fulin Zhang , Huimin Hao, Xiaoyun Dong, Xia Li, Xianjun Lang[*]

Sauvage Center for Molecular Sciences and Hubei Key Lab on Organic and Polymeric Optoelectronic Materials, College of Chemistry and Molecular Sciences, Wuhan University, Wuhan 430072, China

A B S T R A C T

Imine, hydrazone, and olefin-linked covalent organic frameworks (COFs) prosper in visible light photocatalysis. Markedly, the olefin-linked COFs are usually superior in transfer of π-conjugated electron powered by visible light albeit their construction is more challenging. Herein, two olefin-linked COFs were forged between 2,4,6-tri-methyl-1,3,5-triazine (TMT) and 2,4,6-tris(4-formyl-phenyl)-1,3,5-triazine (TFPT) or 1,3,5-tris(4-formyl-phenyl)-benzene (TFPB) to afford TTO-COF or TBO-COF, respectively. Both of the olefin-linked COFs based on triazine are of good crystallinity, uniform micropores, and high specific surface areas, but of different morphologies, namely nanotubes and nanosheets. Compared to TBO-COF, TTO-COF nanotubes were constructed with two building blocks based on triazine, which could not only improve the planarity of a single layer but also cause closer stacking of layers in between. Therefore, TTO-COF nanotubes exhibit better photocatalytic performance and stability in the selective oxidation of organic sulfides into corresponding sulfoxides with O_2 powered by blue light. Mechanistic investigation evidence the formation of desired sulfoxides was shaped by both electron and energy transfer pathways over TTO-COF nanotubes. This work underlines the ascendancy of olefin-linked COFs inasmuch as they provide an effective platform to construct efficient and durable photo-catalysts based on adaptable organic building blocks.

1. Introduction

COFs, constructed with covalent bond-linked repeating organic units of long-range ordered structures, inherent porosity, and tunable properties [1,2], have exhibited potential applicability in gas separation [3, 4], energy storage [5,6], drug delivery [7], and electrocatalysis [8,9], attracting expanding attention. Distinctly, a multitude of COFs with semiconducting properties have served as excellent visible light photo-catalysts for the splitting of water [10,11], reduction of CO_2 [12,13], degradation of pollutants [14,15], and transformation of organics [16, 17], which are efficient to utilize and store solar energy [18]. Organic transformation powered by visible light is a major element of sustainable solar energy utilization [19–21] in which semiconducting COFs could play a pivotal role. However, considerable imine and hydrazone-linked COFs [22–24] exhibit a low degree of π-electron delocalization and structural stability, seriously obstructing their development as organic semiconductors. In stark contrast, olefin has higher bond energy and more fully conjugated electrons that lead to better stability and excellent electron transfer efficiency [25–27], which

are vital properties for photocatalysts [28]. Nevertheless, the construction of olefin-linked COFs is extremely challenging due to the low reversibility of olefin bond. Encouragingly, several cyano-substituted sp^2 carbon-conjugated COFs via Knoevenagel condensation have been reported recently with outstanding photocatalytic activity [29–32]. Meanwhile, another kind of sp^2 carbon-conjugated COFs connected by unsubstituted olefin linkages have been constructed through condensation between activated methyl groups of electron-deficient mesitylene monomers and aryl aldehydes [33–35], which could possess more complete conjugacy of the planar molecule linked by non-polar olefin.

Miscellaneous polymers and molecules based on triazine, a planar molecule with efficient π-electron transport and multiple pyridinic nitrogen atoms, have been extensively applied in the storage and utilization of solar energy, such as organic solar cells [36], optoelectronic materials [37], and photocatalysis [38–41]. And also, triazine plays an important role in enhancing the structural stability due to the planar structure with weaker steric hindrance than a benzene ring [42,43], which benefits the charge carrier mobility of the photocatalytic materials, and accommodates the construction of composites with other

---

semiconductor materials [44–46]. Moreover, triazine, as the photo-active and light-harvesting center, attracts considerable interest to the design of conjugated organic polymer photocatalysts, such as covalent triazine frameworks [47,48] and conjugated COFs [49–51]. Meanwhile, triazine could act as an electron acceptor group to construct the donor−acceptor systems with other electron donors, boosting the separation of photo-generated holes and electrons [52,53].

Therefore, constructing the olefin-linked COFs based on triazine might be a viable strategy to obtain stable and efficient photocatalysts [54]. Recently, two triazine-cored COFs with olefin linkages were reported, possessing high crystallinity and photocatalytic hydrogen evolution activity [55]. Moreover, an olefin-linked 2D COF based on triazine was constructed via organic acid catalyzed condensation to conduct the photocatalytic reduction of uranium [56]. The effectiveness of olefin-linked COFs could be confirmed by these outstanding precedents. Fundamentally, the effects of unsubstituted olefin linkages and the proportion of triazine units in COFs on structural stability and photocatalytic activity are extremely valuable to design durable and efficient COF photocatalysts.

Herein, two olefin-linked COFs, namely TTO-COF and TBO-COF, were constructed with different building blocks based on triazine via condensation catalyzed by an organic acid and an inorganic base, respectively. Structural characterizations reveal their highly crystalline microporous structures with high specific surface areas; and electron microscopy images show nanotubes and scaly stacking nanosheets morphologies of TTO-COF and TBO-COF. As expected, both of them displayed excellent visible light absorption capacity and photocatalytic activity. Interestingly, TTO-COF nanotubes possess superior activity, stability, and durability for selective oxidation of sulfides with O_2 powered by blue light, owing to more efficient charge carrier separation and mobility from the better crystallinity and more salient chemical structures of the two building blocks based on triazine. This work foreshadows that exquisite nanostructures could be built upon olefin-linked COFs to harness visible light for multifarious organic transformations.

2. Experimental section

2.1. Synthesis of TTO-COF

TTO-COF was synthesized according to a prior report with some modifications [38]. Trifluoroacetic acid (TFA), a strong organic acid, was utilized to accelerate the aldol condensation between TMT and TFPT. And mesitylene and dioxane were mixed to regulate the polarity of the reaction system. Then, after continuous optimum condition, TTO-COF with high crystallinity was synthesized successfully. In detail, a 20 mL quartz tube was charged with 38.52 mg TFPT (0.1 mmol) and 12.30 mg TMT (0.1 mmol), then the 1.0 mL mesitylene, 1.0 mL 1, 4-dioxane, and 0.4 mL TFA were added into this tube in sequence. The tube was sonicated for 3 min and sealed by flame after three freeze-pump-thaw cycles. The mixture was heated up to 150 °C and kept for 72 h, yielding precipitate which was isolated by filtration, washed with acetone, methanol three times, then evacuated under vacuum at 100 °C for 12 h to yield activated TTO-COF.

2.2. Synthesis of TBO-COF

TBO-COF was synthesized according to a prior report with some modifications [55]. In detail, a 20 mL quartz tube was charged with 39.04 mg TFPB (0.1 mmol), 12.30 mg TMT (0.1 mmol), 16.83 mg potassium hydroxide (0.3 mmol), and the 1.4 mL *n*-butanol (*n*BuOH) and 0.6 mL 1,2-dichlorobenzene (*o*-DCB) were added into this tube in sequence. The tube was sonicated for 3 min and sealed by flame after three freeze-pump-thaw cycles. This mixture was heated up to 120 °C and kept for 72 h. The yielded precipitate was isolated by filtration, washed with acetone, methanol three times, then evacuated under vacuum at 100 °C for 12 h to furnish the activated TBO-COF.

2.3. Typical procedure for selective oxidation of sulfide with O_2 powered by blue light

At first, 5 mg TTO-COF and 0.3 mmol sulfide were added into a 10 mL Pyrex reactor with 1 mL CH_3OH. Secondly, the Pyrex reactor was kept stirring for 0.5 h in the dark to attain sorption equilibrium. Then, after loading 0.1 MPa O_2, the Pyrex reactor was located on magnetic stirring apparatus with a stirring speed of 1500 rpm and was irradiated by blue LEDs (light-emitting diodes, 3 W × 4) at room temperature. The photocatalyst was separated from the reaction mixture by centrifugation. By gas chromatography collocated with a flame ionization detector (GC–FID, Agilent 7890B), the dissociated supernatant was monitored after centrifugation. Finally, the target product was identified by GC–FID and substantiated by gas chromatography–mass spectrometry (GC–MS, Agilent 5977B GC/MSD).

3. Results and discussion

3.1. Characterizations of TTO-COF and TBO-COF

In order to confirm the successful synthesis and explore their chemical structures and properties of TTO-COF and TBO-COF (Fig. 1a), a series of characterizations were subsequently implemented.

The crystallinity of TTO-COF and TBO-COF was assessed by powder X-ray diffraction (PXRD). As shown in Fig. 1b, the diffraction peaks of TTO-COF at 5.9°, 10.3°, 11.9°, 15.4°, and 26.3° are indexed as reflections from the planes (100), (110), (200), (210), and (001), respectively. Analogously, the PXRD pattern of TBO-COF (Fig. 1c) shows five diffraction peaks at 6.0°, 10.2°, 12.0°, 15.4°, and 25.3°, corresponding to reflections from the planes (100), (110), (200), (210), and (001), respectively. Notably, the diffraction peaks at 5.9° is sharp and intense, indicating the high crystallinity of TTO-COF. Moreover, the broad peaks at 26.3° and 25.3° of TTO-COF and TBO-COF correspond to a layer-to-layer spacing of 3.4 Å and 3.5 Å. The crystallinity of TBO-COF was not good enough. To get higher crystalline TBO-COF, optimization of factors like the solvent, temperature, and bases was made many times. However, the promotion was negligible. The nonplanar triphenylbenzene building block in TBO-COF might be the leading cause, making it hard to form stable and orderly frameworks.

Nitrogen sorption experiments at 77 K were utilized to investigate permanent porosities of TTO-COF and TBO-COF (Fig. 1d and e). There is a sharp rise in the adsorption isotherms of both TTO-COF and TBO-COF in the low-pressure region (P/P$_0$ < 0.05), which could be identified as type I sorption isotherm, indicating their microporosity. The specific surface areas of TTO-COF and TBO-COF were calculated as 491.5 m^2 g^{-1} and 603.9 m^2 g^{-1} (Fig. S4, Supplementary Data), with total pore volumes of 0.28 cm^3 g^{-1} and 0.33 cm^3 g^{-1} at P/P$_0$ = 0.95. The pore size distributions were evaluated by non-local density functional theory (NLDFT) models. Prominent distribution peaks at 1.27 nm and 1.18 nm were found for TTO-COF and TBO-COF, respectively.

The scanning electron microscopy (SEM) images of TTO-COF and TBO-COF (Fig. 2a and c) reveal their fibrillar and scaly stacking nanosheet morphologies. According to the transmission electron microscopy (TEM) image of TTO-COF (Fig. 2b), these nanofibers are actually nanotubes with a diameter of ~100 nm and thickness of ~20 nm, which have huge cavities that could be utilized as reaction centers. The layer-layer stacking nanosheets of TBO-COF could be observed clearly in Fig. 2d, corresponding to its morphology in the SEM image. Additionally, The thermogravimetric analysis (TGA) curves of TTO-COF nanotubes and TBO-COF reveal their high thermal stability with more than 80% weight maintenance up to 500 ℃ in an atmosphere of nitrogen (Fig. S3, Supplementary Data).

Furthermore, the chemical structures of TTO-COF nanotubes and TBO-COF were confirmed by Fourier transform infrared (FTIR)
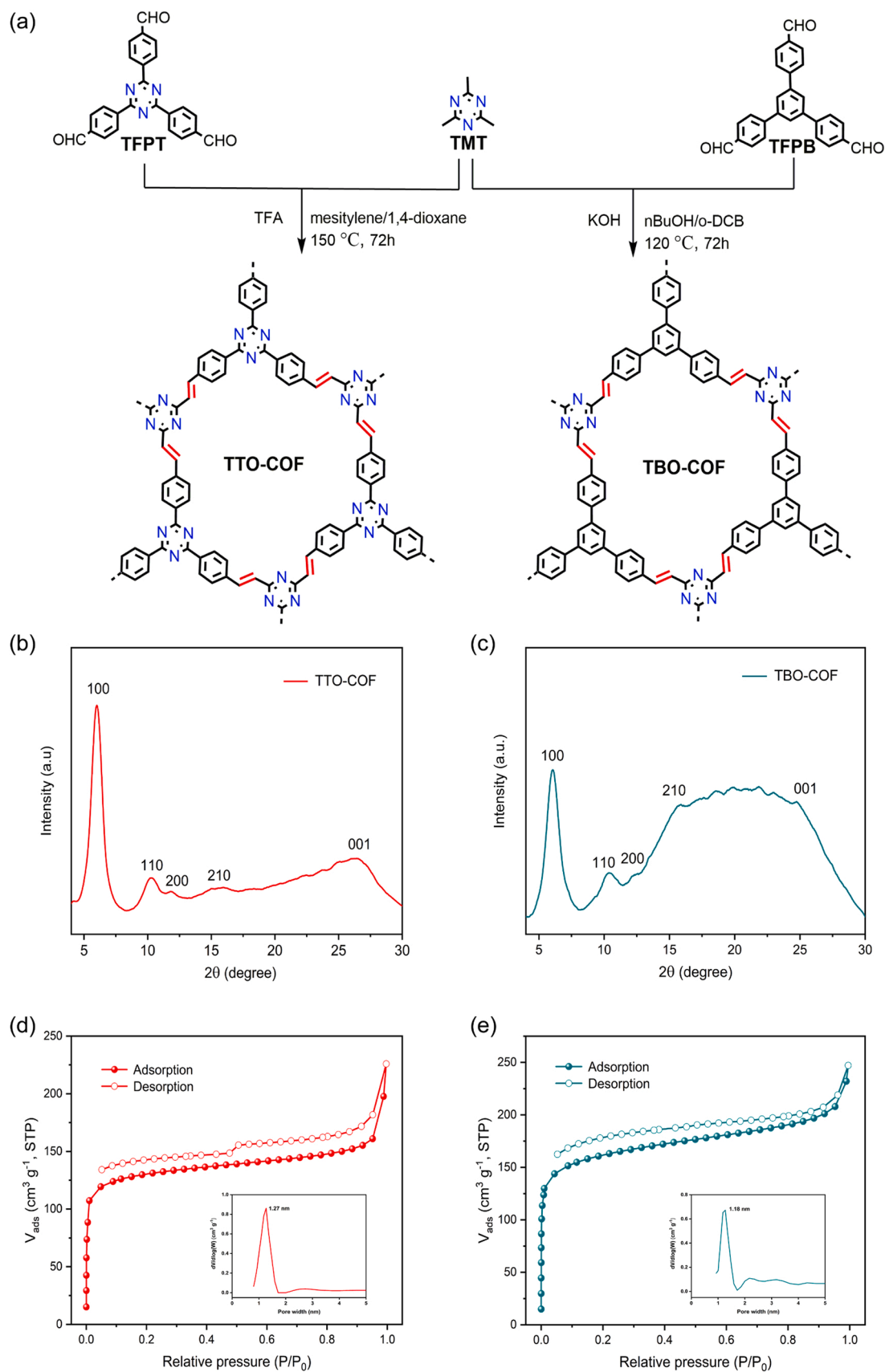
Fig. 1. (a) Synthesis of TTO-COF and TBO-COF; PXRD patterns of TTO-COF (b) and TBO-COF (c); Nitrogen sorption isotherms of TTO-COF (d) and TBO-COF (e). Insets are the pore size distributions calculated from NLDFT.
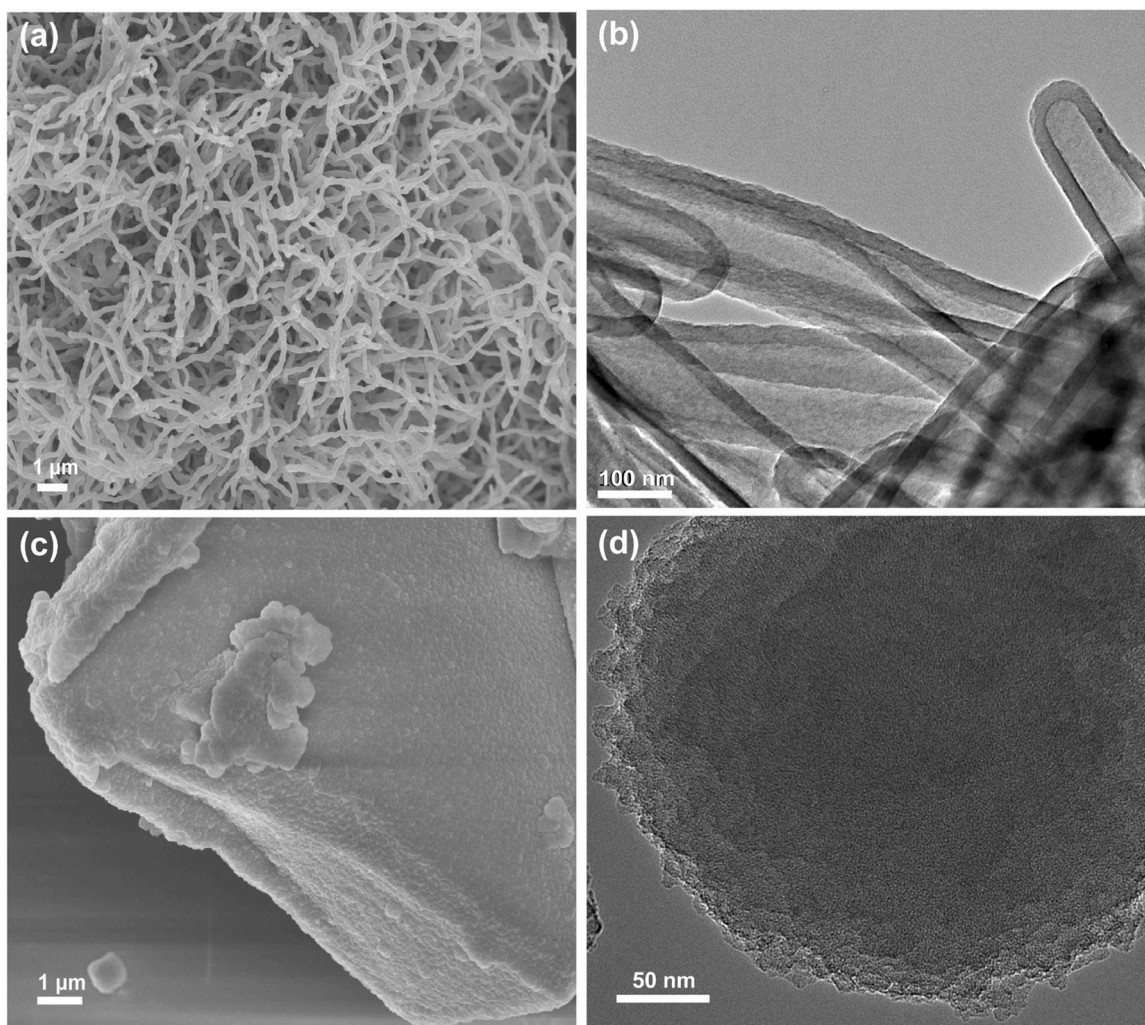
Fig. 2. SEM (a) and TEM (b) images of TTO-COF; SEM (c) and TEM (d) images of TBO-COF.

spectroscopy and solid-state ^{13}C cross-polarization magic angle spinning (CP-MAS) NMR. FTIR spectra of TTO-COF nanotubes, TBO-COF, and their building blocks are shown in Fig. 3a and b. The high-strength peaks at 1511 cm^{-1} correspond to the triazine moiety. The C=O stretching frequency of TFPT at 1704 cm^{-1} almost disappears completely in TTO-COF nanotubes. There is a new absorption peak at 1623 cm^{-1} which corresponds to C=C stretching, indicating the successful formation of the olefin linkages in TTO-COF nanotubes. The C=O stretching frequency of TFPB at 1693 cm^{-1} disappears thoroughly in TBO-COF. At 1633 cm^{-1}, a new absorption peak appears, corresponding to C=C stretching indicated the successful formation of the olefin linkages in TBO-COF. The ^{13}C NMR spectra of TTO-COF nanotubes and TBO-COF are supplied in Fig. S5 (Supplementary Data). Taking the TTO-COF nanotubes as an example, two peaks around 170 ppm are arising from the carbons of triazine. The strong resonance signals between 110 and 150 ppm are attributed to the carbons of olefin linkage and phenylene.

The optical properties of TTO-COF nanotubes and TBO-COF were investigated by ultraviolet−visible diffuse reflectance spectroscopy (UV−vis DRS). There are broad absorption bands with maximum peaks at 400 nm for TTO-COF nanotubes and 420 nm for TBO-COF in their UV−vis DRS (Fig. 3c, d), indicating the strong visible light harvesting. It should be noted that TTO-COF nanotubes possess better absorption at the range of 450–600 nm, likely due to closer π-π stackings. In turn, their optical bandgaps were evaluated to be 2.71 eV for TTO-COF nanotubes and 2.65 eV for TBO-COF from the Kubelka−Munk transformed reflectance spectra. It could be concluded that the increase of the content of

triazine units in COFs would make the optical bandgap wider.

Photoluminescence spectroscopy was utilized to evaluate the charge recombination in both COFs. TTO-COF and TBO-COF had different emission maxima at 513 nm and 542 nm (Fig. S6a, Supplementary Data), respectively. Furthermore, through time-resolved fluorescence decay spectroscopy, the photogenerated charge carrier transfer dynamics of TTO-COF nanotubes and TBO-COF were investigated (Fig. S6b, Supplementary Data). The average lifetimes of TTO-COF nanotubes and TBO-COF excited at 375 nm were calculated to be 4.7 and 2.3 ns, indicating the greatly depressed recombination of photogenerated electrons and holes in TTO-COF nanotubes.

Next, a systematic study of the semiconducting behaviors of the two olefin-linked COFs is necessary. The type of conductivity of TTO-COF nanotubes and TBO-COF was confirmed by Mott−Schottky analysis in an aqueous Na$_2$SO$_4$ solution (0.1 M). The positive slopes of Mott−Schottky plots (Fig. 4a and b) indicate they are both n-type semiconductors. Thus the electrons are the staple charge carriers, consistent with their fully conjugated structures and olefin linkages. And also, the flat-band potential (E_{fb}) of TTO-COF nanotubes and TBO-COF can be fitted to be −1.30 V and −1.16 V vs. Ag/AgCl respectively according to their Mott−Schottky plots. Considering the flat-band potential of an n-type organic semiconductor is close to its lowest unoccupied molecular orbital (LUMO), the highest occupied molecular orbital (HOMO) of TTO-COF nanotubes and TBO-COF can be acquired as 1.41 eV and 1.49 eV. Notably, the photocurrent intensity of TTO-COF nanotubes is almost twice stronger than that of TBO-COF (Fig. 4c), indicative of the more
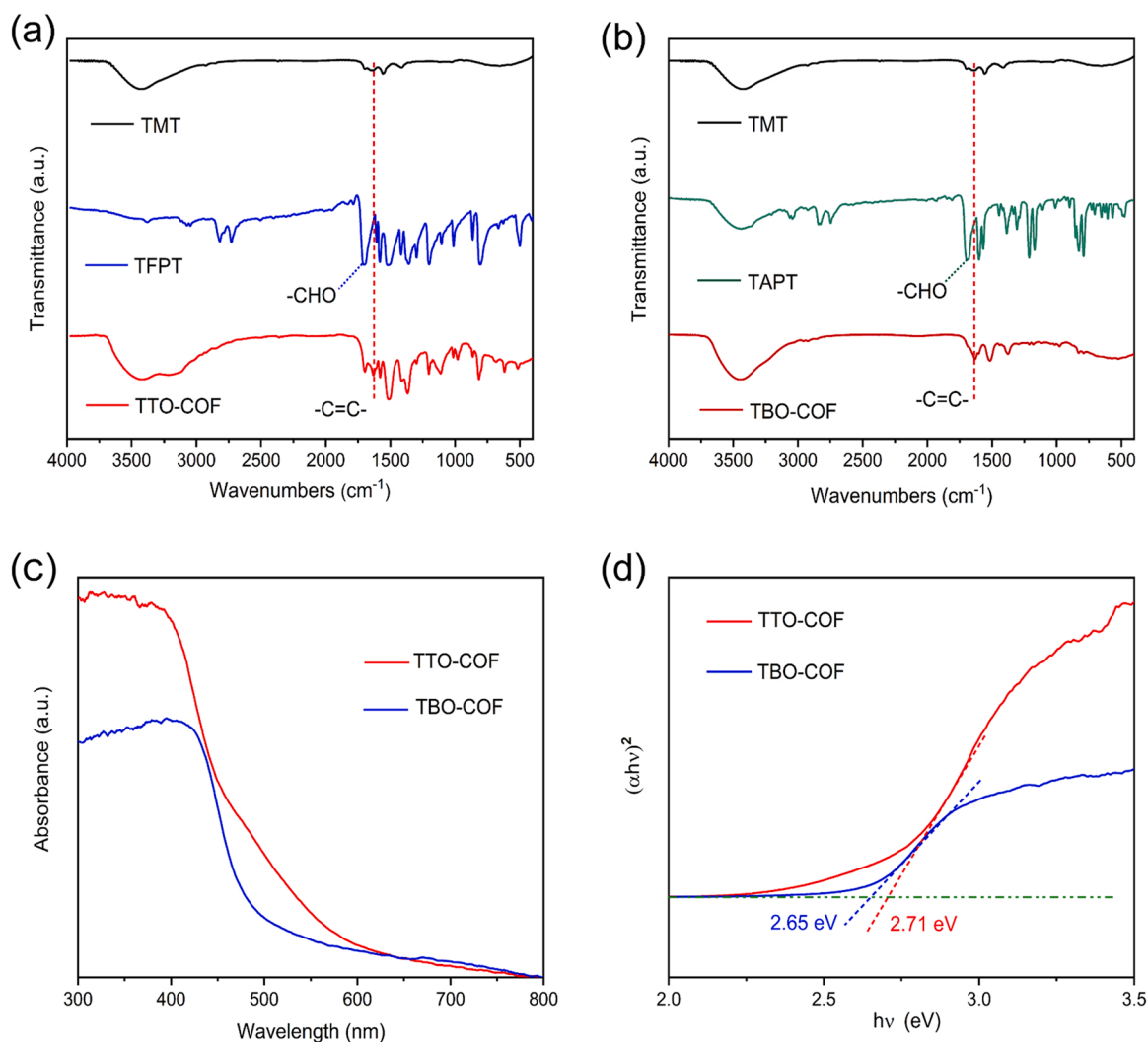
Fig. 3. (a) FTIR spectra of TTO-COF nanotubes and corresponding building blocks; (b) FTIR spectra of TBO-COF and corresponding building blocks; (c) UV–vis DRS spectra of TTO-COF nanotubes and TBO-COF; (d) Optical bandgaps confirmed by the Kubelka–Munk transformed reflectance spectra.

effective separation and mobility of electron/hole in TTO-COF nanotubes. In Nyquist plots (Fig. 4d), TTO-COF nanotubes show a semicircle with a smaller arc radius, indicating the quicker interfacial charge transfer rate and the smaller resistance. These differences in the semiconducting properties of TTO-COF nanotubes and TBO-COF derive from their crystallinities and intrinsic chemical structures, which are related closely to the different building blocks based on triazine in them. Arguably, TTO-COF nanotubes could more probably exhibit better photocatalytic activity.

3.2. Selective oxidation of organic sulfide with O_2 powered by blue light

After these characterizations, it could be confirmed that these two olefin-linked COFs based on triazine have stupendous potential in solar organic conversion. The aerobic oxidation of sulfides to sulfoxides is of great importance in organic synthesis [57,58]. To achieve a better understanding of the difference in their photocatalytic performances, selective oxidation of sulfide was applied to appraise the two olefin-linked COFs.

According to photocatalytic experiments, both of them could transform selectively methyl phenyl sulfide into methyl phenyl sulfoxide with O_2 powered by blue light. Importantly, TTO-COF nanotubes exhibited

more excellent photocatalytic activity than TBO-COF (Fig. S7, Supplementary Data). In detail, 90% of methyl phenyl sulfide could be transformed into methyl phenyl sulfoxide over TTO-COF nanotubes within 2.0 h, which is significantly better than that over TBO-COF (37%). Interestingly, under the irradiation of 460 nm blue LEDs, the yellow color of pristine TBO-COF faded gradually and almost turned white, corresponding to a swift decrease of reaction rate of TBO-COF (Fig. S7, Supplementary Data). It could be known that most of the olefin linkages in the TBO-COF disappeared observed from its FTIR spectra (Fig. S8b, Supplementary Data) after completing the photocatalytic test. The instability is an important reason for the poor photocatalytic efficiency of TBO-COF. The drastically better photocatalytic performance of TTO-COF nanotubes benefits from higher crystallinity, larger specific surface area, better light stability, and closer π-π stacking. Besides, more efficient separation and migration of charge carriers, and the depressed recombination of photogenerated electrons and holes in TTO-COF nanotubes could also promote the selective oxidation of methyl phenyl sulfide.

Different peak wavelengths LEDs were used to confirm the most suitable light source for selective oxidation of sulfide with O_2 over TTO-COF nanotubes (Fig. 5a). The results show that TTO-COF nanotubes possessed the highest conversion (98%) under the irradiation of violet
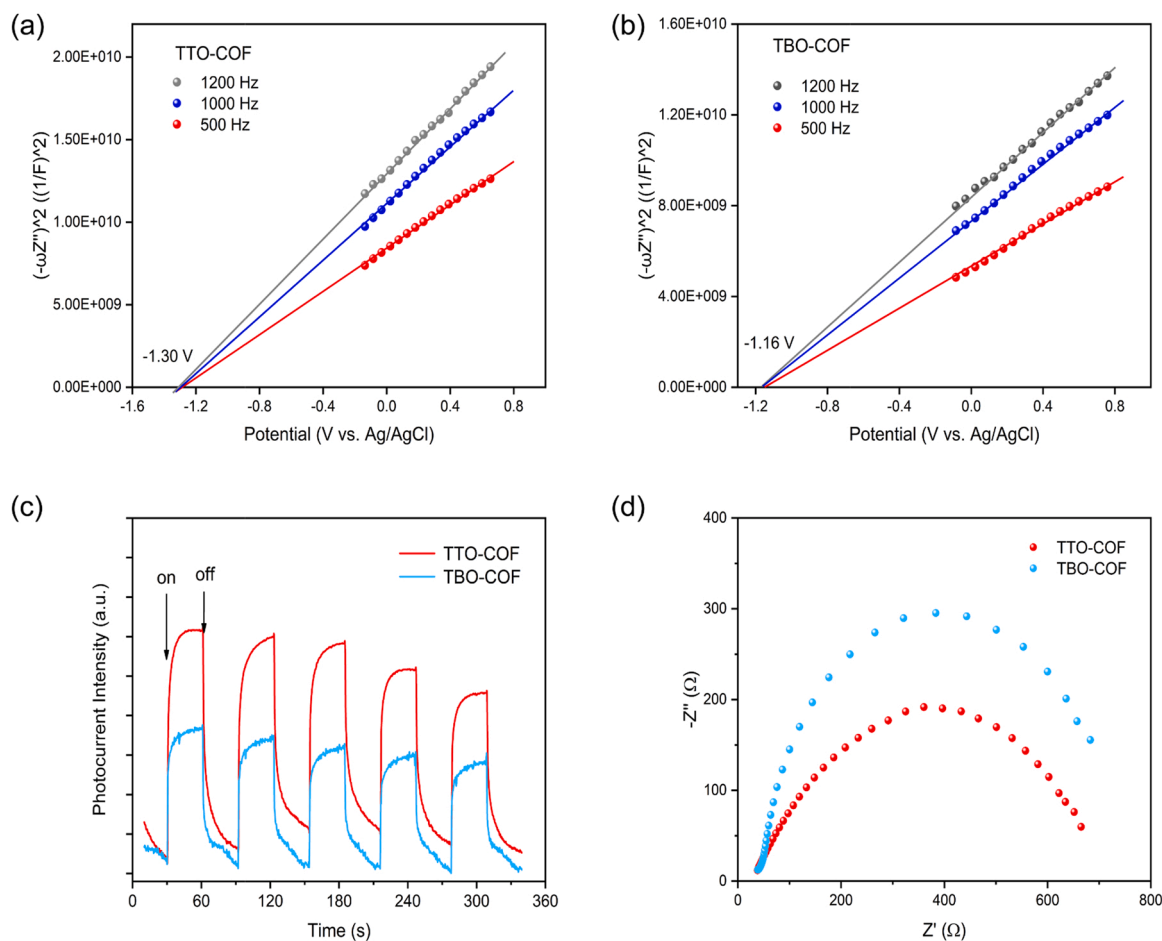
Fig. 4. Mott–Schottky plots of TTO-COF nanotubes (a) and TBO-COF (b) at frequencies of 500, 1000, and 1200 Hz; (c) Photocurrent density vs time of TTO-COF nanotubes and TBO-COF; (d) Electrochemical impedance spectroscopy (EIS) of TTO-COF nanotubes and TBO-COF in the dark.
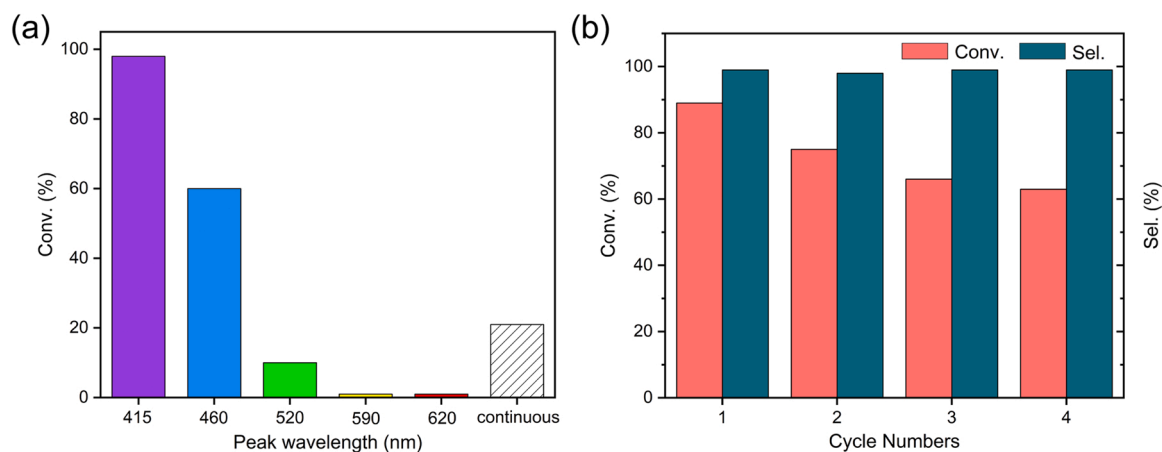

Fig. 5. (a) Different peak wavelengths of LEDs for the selective oxidation of methyl phenyl sulfide into sulfoxide with O_2 over TTO-COF nanotubes; (b) Recycling tests of TTO-COF nanotubes for the selective oxidation of sulfides with O_2 powered by blue light. Reaction conditions: methyl phenyl sulfide (0.3 mmol), TTO-COF nanotubes (5 mg), CH_3OH (1 mL), LEDs (3 W × 4), O_2 (0.1 MPa), (a) 1.0 h, (b) 2.0 h. The conversion of methyl phenyl sulfoxide was determined by GC–FID using bromobenzene as the internal standard.

LEDs in 1.0 h. However, under the 415 nm violet light irradiation, the yellow color of TTO-COF nanotubes faded quickly, indicating an irreversible structural change within TTO-COF nanotubes. Thus, to maintain their structural stability as much as possible, 460 nm blue light is the most suitable light source for the selective oxidation of sulfide with O_2 over TTO-COF nanotubes. Also, the durability of TTO-COF nanotubes

as a heterogeneous photocatalyst was judged by recycling experiments (Fig. 5b). Until the fourth photocatalytic experiment, the conversion for the selective oxidation of methyl phenyl sulfide with O_2 remained above 60%, indicating the durability and effectiveness of TTO-COF nanotubes. The decrease in conversion might be related to inevitable weight loss during the recovery of TTO-COF nanotubes.

3.3. Mechanistic study of photocatalytic oxidation of sulfide over TTO-COF nanotubes

After confirming the effectiveness and recyclability of TTO-COF nanotubes on the selective oxidation of methyl phenyl sulfoxide with O_2, kinetic studies were carried out to acquire more understanding on the preliminary reaction mechanism. According to the kinetic study, the process of reaction accords with the pseudo-first order reaction kinetics. The reaction rate is controlled by the concentration of substrate. The reaction rates in CH_3OH and CD_3OD were computed as 0.01756 mol·L^{-1}·min^{-1} and 0.02675 mol·L^{-1}·min^{-1} (Fig. 6a). It is well known that CD_3OD can maintain the singlet oxygen ($^1O_2$), promoting its lifetime. Thus, the higher reaction rate in CD_3OD indicates that $^1O_2$ participates in the formation of methyl phenyl sulfoxide. In some circumstances, $^1O_2$ could react with olefin, destroying the chemical structure of materials. However, TTO-COF nanotubes displayed excellent stability in the oxidation of sulfide with the participation of $^1O_2$, which could be associated with its special chemical structure. Olefin linkages substituted with electron-withdrawing groups such as triazine are unlikely to react with $^1O_2$. Moreover, most of the olefin linkages in TTO-COF with π-π stacking structures don't have enough space to react with $^1O_2$. Therefore, there is only a small percentage of olefin linkages on the surface that can be attacked by $^1O_2$.

The determination of reactive oxygen species (ROS) is vital to conjecture the reaction mechanism. Therefore, quenching experiments were utilized to confirm the ROS for the selective formation of methyl phenyl sulfoxide with O_2 over TTO-COF nanotubes (Table 1). At first, when the reaction system was fulfilled with nitrogen, the reaction didn't occur, indicating the indispensability of O_2 (Table 1, Entry 2). Afterward, 1,4-diazabicyclo[2.2.2]octane (DABCO) and *p*-benzoquinone (*p*-

Table 1
Quenching experiments to confirm the ROS for the selective oxidation of methyl phenyl sulfide with O_2 over TTO-COF nanotubes powered by blue light.[a]

Entry	Quencher (equiv.)	Roles	Conv. [%][b]	Sel. [%][b]
1[c]	–	–	90	99
2	N_2 (–)	O_2 replacement	0	–
3	*p*-BQ (0.2)	$O_2^{\bullet-}$ scavenger	22	99
4	DABCO (0.1)	$^1O_2$ scavenger	58	97
5	$AgNO_3$ (1)	electron scavenger	53	98
6	TEMPO (0.02)	redox mediator	91	99

[a] Reaction conditions: methyl phenyl sulfide (0.3 mmol), TTO-COF nanotubes (5 mg), CH_3OH (1 mL), blue LEDs (3 W × 4), O_2 (0.1 MPa), 2.0 h.
[b] Determined by GC–FID using bromobenzene as the internal standard, conversion of methyl phenyl sulfide, selectivity of methyl phenyl sulfoxide.
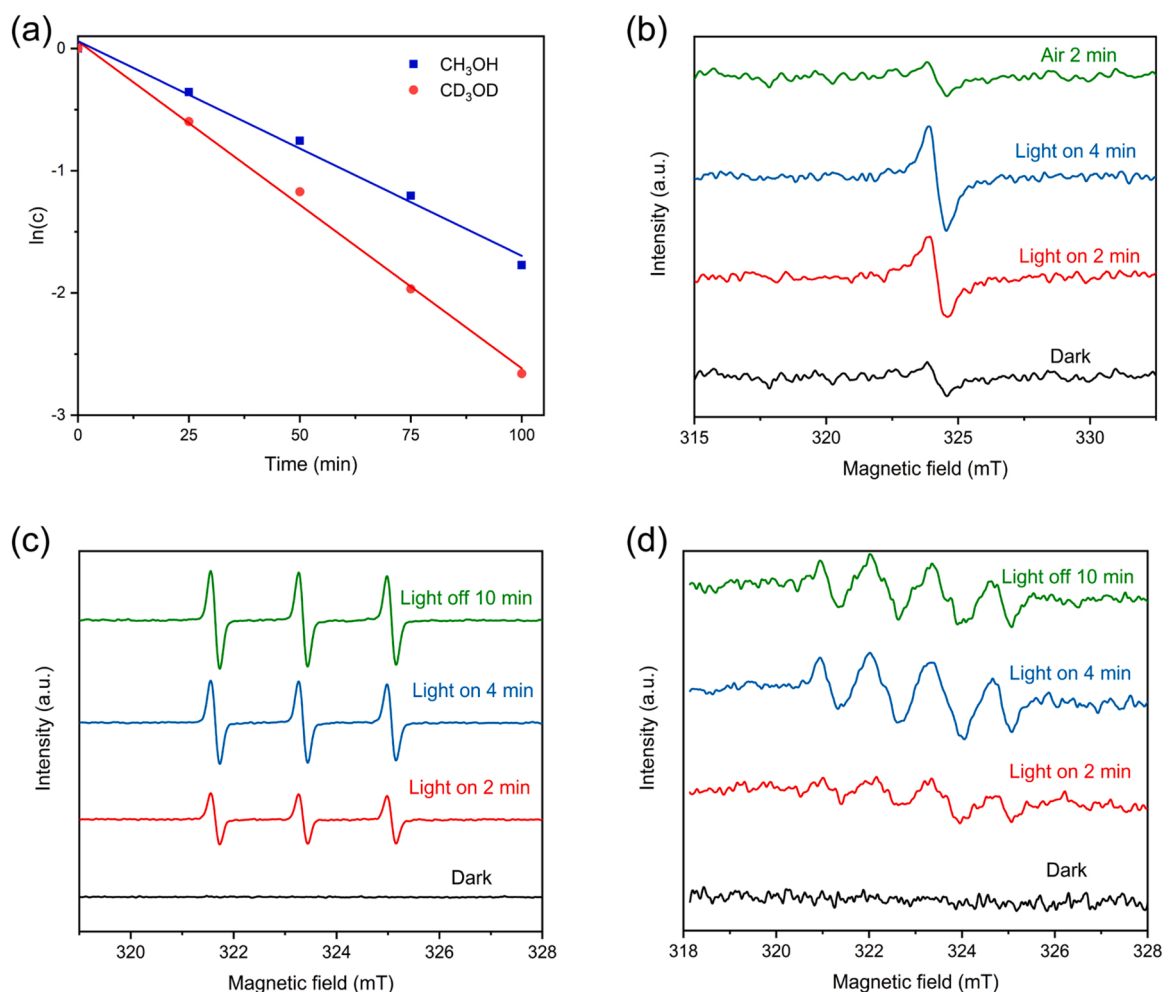[c] Standard reaction conditions.

Fig. 6. (a) Kinetic plots for the selective oxidation of methyl phenyl sulfide with O_2 over TTO-COF nanotubes powered by blue light in CH_3OH and CD_3OD; The EPR spectra of (b) Electrons; (c) Spin trapping of $^1O_2$ with TMPD; (d) Spin trapping of $O_2^{\bullet-}$ with DMPO in the selective oxidation of methyl phenyl sulfide with O_2 over TTO-COF nanotubes powered by blue light.

BQ) were used to capture the $^1O_2$ and $O_2^{\bullet-}$, respectively. And the conversions of methyl phenyl sulfide had varying degrees of reduction (Table 1, Entries 3 and 4), demonstrating the existence of $O_2^{\bullet-}$ and $^1O_2$ in the reaction progress. The selective oxidation occurred in CH_3OH that can quench any readily generated hydroxyl radical. Therefore, one can rule out the role of hydroxyl radicals in the oxidation of sulfide. Also, when one equivalent of $AgNO_3$ was added into the reaction system as an electron scavenger, the reaction was inhibited (Table 1, Entry 5), which is ascribed to the delaying electrons transfer in the oxidation. Then TEMPO was added to the reaction system as a redox mediator (Table 1, Entry 6), while the catalytic effect was inconspicuous.

Routinely, electron paramagnetic resonance (EPR) is a useful tool to study unpaired electron spins. Therefore, it was utilized to record signals of different ROS to assist the deduction of the reaction mechanism. As shown in Fig. 6b, when electrons on the HOMO of TTO-COF nanotubes were excited to the LUMO powered by blue light, the detected signals of electrons increased continuously with consequent irradiation. Nevertheless, when air was introduced into the reaction system, the signals of electrons decreased sharply, indicating the combination of electrons and O_2. The $O_2^{\bullet-}$ and $^1O_2$ were trapped by 5,5-dimethyl-1-pyrroline *N*-oxide (DMPO) and 2,2,6,6-tetramethyl-4-piperidone (TMPD), respectively. Their EPR signals (Fig. 6c and d) could also confirm that both $O_2^{\bullet-}$ and $^1O_2$ participate in the photocatalytic selectively oxidation of sulfides. In general, the photocatalytic conversion of sulfides to corresponding sulfoxides has two pathways including electron transfer and energy transfer.

In consequence, a tentative mechanism for the photocatalytic oxidation of methyl phenyl sulfide over TTO-COF nanotubes is depicted in Fig. 7. There are two pathways including electron transfer and energy transfer in the photocatalytic oxidation of sulfide over TTO-COF nanotubes. Powered by blue light, charge separation takes place in TTO-COF nanotubes. In the electron transfer pathway, methyl phenyl sulfide is oxidized to the corresponding cationic radical by photogenerated holes; and the O_2 is reduced to $O_2^{\bullet-}$ by photogenerated electrons in the LUMO of TTO-COF nanotubes. Finally, the $O_2^{\bullet-}$ reacts with the cationic radical intermediate, forming the persulfoxide which transforms into the final methyl phenyl sulfoxide with the cooperation of protons from CH_3OH. In the energy transfer pathway, O_2 is converted into $^1O_2$ through triplet-triplet annihilation between the triplet excited state of TTO-COF nanotubes and $^3O_2$. Then methyl phenyl sulfide will be further oxidized to persulfoxide by $^1O_2$. And methyl phenyl sulfoxide is obtained after the similar progress with the cooperation of protons from CH_3OH.

3.4. Scope for the oxidation of sulfides over TTO-COF nanotubes

After confirming the effectiveness and recyclability of the TTO-COF nanotubes on the selective oxidation of methyl phenyl sulfide, the scope of the substrates is necessary to be established (Table 2), which is essential for certifying the applicability of the reaction mechanism. Powered by blue light, methyl phenyl sulfide and the majority of its derivatives could be transformed into corresponding sulfoxides efficiently at standard conditions (Table 2, Entries 1–9). Some regular patterns could be observed in the series of experiments of oxidation of sulfides.

Compared to methyl phenyl sulfide, sulfides with electron-donating groups (Table 2, Entries 2 and 5) commonly possessed higher conversions. Conversely, methyl phenyl sulfides with electron-withdrawing groups (Table 2, Entries 3 and 4, 7–10) typically exhibited lower conversions than methyl phenyl sulfide (Table 2, Entry 1). The methyl phenyl sulfide substituted by *para-t*-butyl with a negligible electron effect has a similar conversion at the same time (Table 2, Entry 6). Notably, the methoxy in the *para* position of phenyl behaves as an electron-donating group overall, leading to higher conversion (Table 2, Entry 2). Due to the extremely electron-withdrawing effect, the transformation of the methyl phenyl sulfide substituted by *p*-nitro was restrained seriously (Table 2, Entry 10). Furthermore, *m*- and *o*-substituted chloroanisoles were utilized to investigate the influence of different substituted positions on their conversions. With the decrease of the distance of chlorine and methylthio group, the electron-withdrawing effect becomes stronger, and the conversions of substrates were lower (Table 2, Entries 8, 11 and 12). When the methyl group was substituted with an ethyl group, the conversion of sulfide decreased slightly (Table 2, Entry 13). And when the methyl group was substituted with phenyl, the reaction almost didn't occur (Table 2, Entry 14), demonstrating the significant influence of the steric hindrance effect. Interestingly, the photocatalytic formation of aliphatic sulfoxides (Table 2, Entries 15 and 16) was also feasible and exhibited higher efficiency.
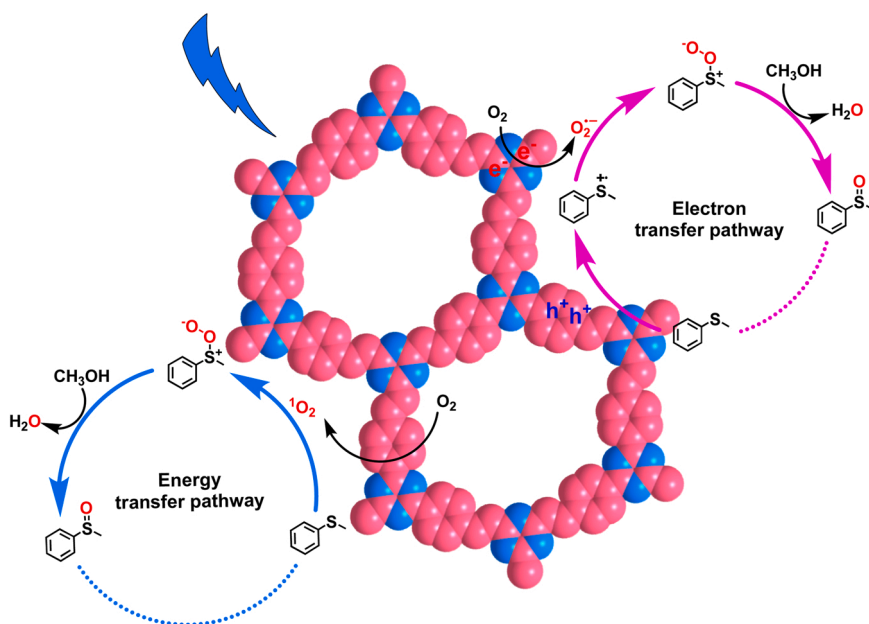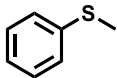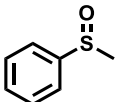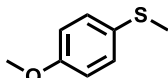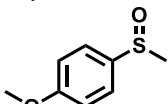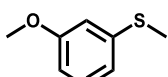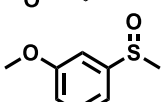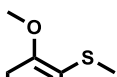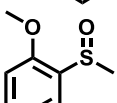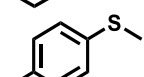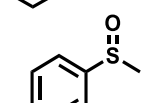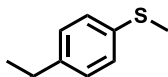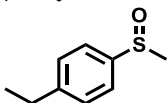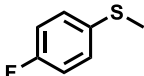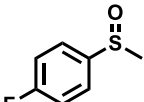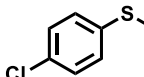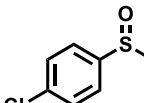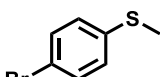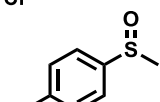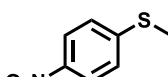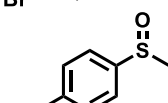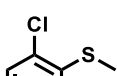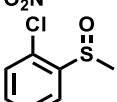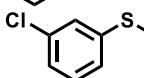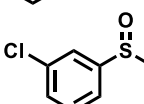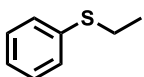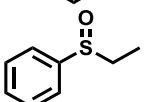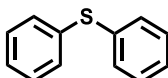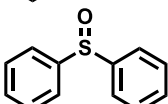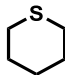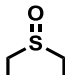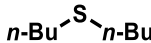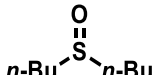

Fig. 7. The proposed mechanism for the selective oxidation of methyl phenyl sulfide with O_2 over TTO-COF nanotubes powered by blue light.

Table 2

The selective oxidation of sulfides with O_2 over TTO-COF nanotubes powered by blue light.[a]

Entry	Substrate	Product	t (h)	Conv. (%)[b]	Sel. (%)[b]
1			2.0	90	98
2			2.0	98	99
3			2.0	84	98
4			2.0	82	99
5			2.0	94	97
6			2.0	88	99
7			2.0	84	99
8			2.0	73	99
9			2.0	79	98
10			2.0	21	99
11			2.0	38	99
12			2.0	47	99
13			2.0	77	99
14			2.0	6	99

Table 2 (*continued*)

Entry	Substrate	Product	t (h)	Conv. (%)[b]	Sel. (%)[b]
15			1.0	98	96
16	*n*-Bu-S-*n*-Bu		1.0	99	96

[a] Reaction conditions: sulfide (0.3 mmol), TTO-COF nanotubes (5 mg), CH_3OH (1 mL), blue LEDs (3 W × 4), O_2 (0.1 MPa).

[b] Determined by GC–FID using bromobenzene as the internal standard, conversion of sulfide, selectivity of sulfoxide.

4. Conclusions

In summary, two olefin-linked COFs based on triazine have been synthesized successfully. Thereafter, their structural and photoelectronic attributes have been characterized thoroughly. The TTO-COF nanotubes, constructed with two building blocks based on triazine, turned out to be a superior photocatalyst to TBO-COF for selective oxidation of sulfides with O_2 powered by blue light. The higher crystallinity and particular morphology of TTO-COF nanotubes have endowed more efficient separation and mobility of charge carriers, lower recombination of electrons and holes, and therefore better activity. Significantly, the introduction of planar and fully conjugated triazine units could promote the crystallinity and stability of COFs and modify their photoelectric properties. Mechanistic investigations evidence that the selective formation of desired sulfoxides over TTO-COF nanotubes is shaped by both electron and energy transfer pathways. This work underlines the ascendancy of olefin-linked COFs in multifarious organic transformation inasmuch as they provide an effective platform to construct efficient and durable photocatalysts.

CRediT authorship contribution statement

Fulin Zhang: Investigation, Writing – original draft. **Huimin Hao**: Investigation, Formal analysis. **Xiaoyun Dong**: Formal analysis. **Xia Li**: Formal analysis. **Xianjun Lang**: Conceptualization, Supervision, Writing – review & editing and Funding acquisition.

Declaration of Competing Interest

The authors declare that they have no known competing financial interests or personal relationships that could have appeared to influence the work reported in this paper.

Acknowledgements

Appendix A. Supporting information

Supplementary data associated with this article can be found in the online version at doi:10.1016/j.apcatb.2021.121027.

References

[1] K.Y. Geng, T. He, R.Y. Liu, S. Dalapati, K.T. Tan, Z.P. Li, S.S. Tao, Y.F. Gong, Q. H. Jiang, D.L. Jiang, Covalent organic frameworks: Design, synthesis, and functions, Chem. Rev. 120 (2020) 8814–8933, https://doi.org/10.1021/acs. chemrev.9b00550.

[2] M.S. Lohse, T. Bein, Covalent organic frameworks: Structures, synthesis, and applications, Adv. Funct. Mater. 28 (2018), 1705553, https://doi.org/10.1002/ adfm.201705553.

[3] H.W. Fan, M.H. Peng, I. Strauss, A. Mundstock, H. Meng, J. Caro, High-flux vertically aligned 2D covalent organic framework membrane with enhanced hydrogen separation, J. Am. Chem. Soc. 142 (2020) 6872–6877, https://doi.org/ 10.1021/jacs.0c00927.

[4] C.H. Ma, X.L. Li, J. Zhang, Y. Liu, J.J. Urban, Pyrazine-fused porous graphitic framework-based mixed matrix membranes for enhanced gas separations, ACS Appl. Mater. Interfaces 12 (2020) 16922–16929, https://doi.org/10.1021/ acsami.0c01378.

[5] D.G. Wang, T.J. Qiu, W.H. Guo, Z.B. Liang, H. Tabassum, D.G. Xia, R.Q. Zou, Covalent organic framework-based materials for energy applications, Energy Environ. Sci. 14 (2021) 688–728, https://doi.org/10.1039/d0ee02309d.

[6] Y. Yusran, Q.R. Fang, V. Valtchev, Electroactive covalent organic frameworks: Design, synthesis, and applications, Adv. Mater. 32 (2020), 2002038, https://doi. org/10.1002/adma.202002038.

[7] L. Ge, C.Y. Qiao, Y.K. Tang, X.K. Zhang, X.Q. Jiang, Light-activated hypoxia-sensitive covalent organic framework for tandem-responsive drug delivery, Nano Lett. 21 (2021) 3218–3224, https://doi.org/10.1021/acs.nanolett.1c00488.

[8] J. Li, X.C. Jing, Q.Q. Li, S.W. Li, X. Gao, X. Feng, B. Wang, Bulk COFs and COF nanosheets for electrochemical energy storage and conversion, Chem. Soc. Rev. 49 (2020) 3565–3604, https://doi.org/10.1039/d0cs00017e.

[9] X. Cui, S. Lei, A.C. Wang, L.K. Gao, Q. Zhang, Y.K. Yang, Z.Q. Lin, Emerging covalent organic frameworks tailored materials for electrocatalysis, Nano Energy 70 (2020), 104525, https://doi.org/10.1016/j.nanoen.2020.104525.

[10] X.Y. Wang, L.J. Chen, S.Y. Chong, M.A. Little, Y.Z. Wu, W.H. Zhu, R. Clowes, Y. Yan, M.A. Zwijnenburg, R.S. Sprick, A.I. Cooper, Sulfone-containing covalent organic frameworks for photocatalytic hydrogen evolution from water, Nat. Chem. 10 (2018) 1180–1189, https://doi.org/10.1038/s41557-018-0141-5.

[11] T. Banerjee, F. Haase, G. Savasci, K. Gottschling, C. Ochsenfeld, B.V. Lotsch, Single-site photocatalytic H₂ evolution from covalent organic frameworks with molecular cobaloxime co-catalysts, J. Am. Chem. Soc. 139 (2017) 16228–16234, https://doi. org/10.1021/jacs.7b07489.

[12] S.Z. Yang, W.H. Hu, X. Zhang, P.L. He, B. Pattengale, C.M. Liu, M. Cendejas, I. Hermans, X.Y. Zhang, J. Zhang, J.E. Huang, 2D covalent organic frameworks as intrinsic photocatalysts for visible light-driven CO₂ reduction, J. Am. Chem. Soc. 140 (2018) 14614–14618, https://doi.org/10.1021/jacs.8b09705.

[13] W.F. Zhong, R.J. Sa, L.Y. Li, Y.J. He, L.Y. Li, J.H. Bi, Z.Y. Zhuang, Y. Yu, Z.G. Zou, A covalent organic framework bearing single Ni sites as a synergistic photocatalyst for selective photoreduction of CO₂ to CO, J. Am. Chem. Soc. 141 (2019) 7615–7621, https://doi.org/10.1021/jacs.9b02997.

[14] D.T. Yue, X.F. Qian, M. Kan, M.Y. Fang, J.P. Jia, X.D. Yang, Y.X. Zhao, A metal-free visible light active photo-electro-Fenton-like cell for organic pollutants degradation, Appl. Catal. B: Environ. 229 (2018) 211–217, https://doi.org/ 10.1016/j.apcatb.2018.02.033.

[15] W.R. Cui, C.R. Zhang, W. Jiang, F.F. Li, R.P. Liang, J.W. Liu, J.D. Qiu, Regenerable and stable sp² carbon-conjugated covalent organic frameworks for selective detection and extraction of uranium, Nat. Commun. 11 (2020) 436, https://doi. org/10.1038/s41467-020-14289-x.

[16] J.L. Shi, R.F. Chen, H.M. Hao, C. Wang, X.J. Lang, 2D sp² carbon-conjugated porphyrin covalent organic framework for cooperative photocatalysis with TEMPO, Angew. Chem. Int. Ed. 59 (2020) 9088–9093, https://doi.org/10.1002/ anie.202000723.

[17] P.F. Wei, M.Z. Qi, Z.P. Wang, S.Y. Ding, W. Yu, Q. Liu, L.K. Wang, H.Z. Wang, W. K. An, W. Wang, Benzoxazole-linked ultrastable covalent organic frameworks for photocatalysis, J. Am. Chem. Soc. 140 (2018) 4623–4631, https://doi.org/ 10.1021/jacs.8b00571.

[18] H. Wang, H. Wang, Z.W. Wang, L. Tang, G.M. Zeng, P. Xu, M. Chen, T. Xiong, C. Y. Zhou, X.Y. Li, D.N. Huang, Y. Zhu, Z.X. Wang, J.W. Tang, Covalent organic framework photocatalysts: Structures and applications, Chem. Soc. Rev. 49 (2020) 4135–4165, https://doi.org/10.1039/d0cs00278j.

[19] X.J. Lang, J.C. Zhao, X.D. Chen, Visible-light-induced photoredox catalysis of dye-sensitized titanium dioxide: Selective aerobic oxidation of organic sulfides, Angew. Chem. Int. Ed. 55 (2016) 4697–4700, https://doi.org/10.1002/anie.201600405.

[20] H.M. Hao, J.L. Shi, H. Xu, X. Li, X.J. Lang, *N*-hydroxyphthalimide-TiO₂ complex visible light photocatalysis, Appl. Catal. B: Environ. 246 (2019) 149–155, https://doi.org/10.1016/j.apcatb.2019.01.037.

[21] H. Liu, X.L. Yan, W.B. Chen, Z. Xie, S. Li, W.H. Chen, T. Zhang, G.L. Xing, L. Chen, Donor-acceptor 2D covalent organic frameworks for efficient heterogeneous photocatalytic α-oxyamination, Sci. China Chem. 64 (2021) 827–833, https://doi.org/10.1007/s11426-020-9931-4.

[22] W.T. Liu, Q. Su, P.Y. Ju, B.X. Guo, H. Zhou, G.H. Li, Q.L. Wu, A hydrazone-based covalent organic framework as an efficient and reusable photocatalyst for the cross-dehydrogenative coupling reaction of *N*-aryltetrahydroisoquinolines, ChemSusChem 10 (2017) 664–669, https://doi.org/10.1002/cssc.201601702.

[23] Y. Li, W.B. Chen, R.D. Gao, Z.Q. Zhao, T. Zhang, G.L. Xing, L. Chen, 2D covalent organic frameworks with built-in amide active sites for efficient heterogeneous catalysis, Chem. Commun. 55 (2019) 14538–14541, https://doi.org/10.1039/c9cc07500c.

[24] I. Romero-Muñiz, A. Mavrandonakis, P. Albacete, A. Vega, V. Briois, F. Zamora, A.E. Platero-Prats, Unveiling the local structure of palladium loaded into imine-linked layered covalent organic frameworks for cross-coupling catalysis, Angew. Chem. Int. Ed. 59 (2020) 13013–13020, https://doi.org/10.1002/anie.202004197.

[25] N. Keller, T. Bein, Optoelectronic processes in covalent organic frameworks, Chem. Soc. Rev. 50 (2021) 1813–1845, https://doi.org/10.1039/d0cs00793e.

[26] T. He, K.Y. Geng, D.L. Jiang, All sp² carbon covalent organic frameworks, Trends Chem. 3 (2021) 431–444, https://doi.org/10.1016/j.trechm.2021.03.008.

[27] M. Tian, Y.C. Wang, X.B. Bu, Y.C. Wang, X.B. Yang, An ultrastable olefin-linked covalent organic framework for photocatalytic decarboxylative alkylations under highly acidic conditions, Catal. Sci. Technol. 11 (2021) 4272–4279, https://doi.org/10.1039/d1cy00293g.

[28] X.J. Lang, J.C. Zhao, X.D. Chen, Cooperative photoredox catalysis, Chem. Soc. Rev. 45 (2016) 3026–3038, https://doi.org/10.1039/c5cs00659g.

[29] E.Q. Jin, M. Asada, Q. Xu, S. Dalapati, M.A. Addicoat, M.A. Brady, H. Xu, T. Nakamura, T. Heine, Q.H. Chen, D.L. Jiang, Two-dimensional sp²-carbon-conjugated covalent organic frameworks, Science 357 (2017) 673–676, https://doi.org/10.1126/science.aan0202.

[30] Y.G. Xiang, W.B. Dong, P. Wang, S.Y. Wang, X. Ding, F. Ichihara, Z. Wang, Y. Wada, S.B. Jin, Y.X. Weng, H. Chen, J.H. Ye, Constructing electron delocalization channels in covalent organic frameworks powering CO₂ photoreduction in water, Appl. Catal. B: Environ. 274 (2020), 119096, https://doi.org/10.1016/j.apcatb.2020.119096.

[31] Y.J. Zhao, H. Liu, C.Y. Wu, Z.H. Zhang, Q.Y. Pan, F. Hu, R.M. Wang, P.W. Li, X.W. Huang, Z.B. Li, Fully conjugated two-dimensional sp²-carbon covalent organic frameworks as artificial photosystem I with high efficiency, Angew. Chem. Int. Ed. 58 (2019) 5376–5381, https://doi.org/10.1002/anie.201901194.

[32] H.M. Hao, F.L. Zhang, X.Y. Dong, X.J. Lang, 2D sp² carbon-conjugated triazine covalent organic framework photocatalysis for blue light-induced selective oxidation of sulfides with O₂, Appl. Catal. B: Environ. 299 (2021), 120691, https://doi.org/10.1016/j.apcatb.2021.120691.

[33] A. Acharjya, P. Pachfule, J. Roeser, F.J. Schmitt, A. Thomas, Vinylene-linked covalent organic frameworks by base-catalyzed aldol condensation, Angew. Chem. Int. Ed. 58 (2019) 14865–14870, https://doi.org/10.1002/anie.201905886.

[34] J.S. Xu, C. Yang, S. Bi, W.Y. Wang, Y.F. He, D.Q. Wu, Q.F. Liang, X.C. Wang, F. Zhang, Vinylene-linked covalent organic frameworks (COFs) with symmetry-tuned polarity and photocatalytic activity, Angew. Chem. Int. Ed. 59 (2020) 23845–23853, https://doi.org/10.1002/anie.202011852.

[35] H. Lyu, C.S. Diercks, C.H. Zhu, O.M. Yaghi, Porous crystalline olefin-linked covalent organic frameworks, J. Am. Chem. Soc. 141 (2019) 6848–6852, https://doi.org/10.1021/jacs.9b02848.

[36] N. Chakravarthi, U.K. Aryal, K. Gunasekar, H.Y. Park, Y.S. Gal, Y.R. Cho, S. Il Yoo, M. Song, S.H. Jin, Triazine-based polyelectrolyte as an efficient cathode interfacial material for polymer solar cells, ACS Appl. Mater. Interfaces 9 (2017) 24753–24762, https://doi.org/10.1021/acsami.7b03187.

[37] S.J. Ren, D.L. Zeng, H.L. Zhong, Y.C. Wang, S.X. Qian, Q.A. Fang, Star-shaped donor-π-acceptor conjugated oligomers with 1,3,5-triazine cores: Convergent synthesis and multifunctional properties, J. Phys. Chem. B 114 (2010) 10374–10383, https://doi.org/10.1021/jp104710y.

[38] Y.L. Yang, H.Y. Niu, L. Xu, H. Zhang, Y.Q. Cai, Triazine functionalized fully conjugated covalent organic framework for efficient photocatalysis, Appl. Catal. B: Environ. 269 (2020), 118799, https://doi.org/10.1016/j.apcatb.2020.118799.

[39] H.J. Zhang, X.J. Chen, Z.J. Zhang, K.Y. Yu, W. Zhu, Y.F. Zhu, Highly-crystalline triazine-PDI polymer with an enhanced built-in electric field for full-spectrum photocatalytic phenol mineralization, Appl. Catal. B: Environ. 287 (2021), 119957, https://doi.org/10.1016/j.apcatb.2021.119957.

[40] W.J. Wang, G.Y. Li, T.C. An, D.K.L. Chan, J.C. Yu, P.K. Wong, Photocatalytic hydrogen evolution and bacterial inactivation utilizing sonochemical-synthesized g-C₃N₄/red phosphorus hybrid nanosheets as a wide-spectral-responsive photocatalyst: The role of type I band alignment, Appl. Catal. B: Environ. 238 (2018) 126–135, https://doi.org/10.1016/j.apcatb.2018.07.004.

[41] G.Y. Lin, L. Sun, Q.S. Chen, S.Q. Fang, J.H. Bi, L. Wu, Direct Z-scheme copper cobaltite/covalent triazine-based framework heterojunction for efficient photocatalytic CO₂ reduction under visible light, Sustainable Energy Fuels 5 (2021) 732–739, https://doi.org/10.1039/d0se01504k.

[42] C. Krishnaraj, H.S. Jena, K. Leus, P. Van Der Voort, Covalent triazine frameworks – A sustainable perspective, Green Chem. 22 (2020) 1038–1071, https://doi.org/10.1039/c9gc03482j.

[43] Y.C. Wang, H. Liu, Q.Y. Pan, C.Y. Wu, W.B. Hao, J. Xu, R.Z. Chen, J. Liu, Z.B. Li, Y.J. Zhao, Construction of fully conjugated covalent organic frameworks via facile linkage conversion for efficient photoenzymatic catalysis, J. Am. Chem. Soc. 142 (2020) 5958–5963, https://doi.org/10.1021/jacs.0c00923.

[44] D.H. Xia, W.J. Wang, R. Yin, Z.F. Jiang, T.C. An, G.Y. Li, H.J. Zhao, P.K. Wong, Enhanced photocatalytic inactivation of *Escherichia coli* by a novel Z-scheme g-C₃N₄/m-Bi₂O₄ hybrid photocatalyst under visible light: The role of reactive oxygen species, Appl. Catal. B: Environ. 214 (2017) 23–33, https://doi.org/10.1016/j.apcatb.2017.05.035.

[45] W.J. Wang, T.C. An, G.Y. Li, D.H. Xia, H.J. Zhao, J.C. Yu, P.K. Wong, Earth-abundant Ni₂P/g-C₃N₄ lamellar nanohydrids for enhanced photocatalytic hydrogen evolution and bacterial inactivation under visible light irradiation, Appl. Catal. B: Environ. 217 (2017) 570–580, https://doi.org/10.1016/j.apcatb.2017.06.027.

[46] Z.A. Lan, Y.X. Fang, Y.F. Zhang, X.C. Wang, Photocatalytic oxygen evolution from functional triazine-based polymers with tunable band structures, Angew. Chem. Int. Ed. 57 (2018) 470–474, https://doi.org/10.1002/anie.201710846.

[47] M.Y. Liu, Q. Huang, S.L. Wang, Z.Y. Li, B.Y. Li, S.B. Jin, B. Tan, Crystalline covalent triazine frameworks by in situ oxidation of alcohols to aldehyde monomers, Angew. Chem. Int. Ed. 57 (2018) 11968–11972, https://doi.org/10.1002/anie.201806664.

[48] S.Q. Zhang, G. Cheng, L.P. Guo, N. Wang, B.E. Tan, S.B. Jin, Strong-base-assisted synthesis of a crystalline covalent triazine framework with high hydrophilicity via benzylamine monomer for photocatalytic water splitting, Angew. Chem. Int. Ed. 59 (2020) 6007–6014, https://doi.org/10.1002/anie.201914424.

[49] M. Bhadra, S. Kandambeth, M.K. Sahoo, M. Addicoat, E. Balaraman, R. Banerjee, Triazine functionalized porous covalent organic framework for photo-organocatalytic *E–Z* isomerization of olefins, J. Am. Chem. Soc. 141 (2019) 6152–6156, https://doi.org/10.1021/jacs.9b01891.

[50] L.Q. Xu, S.Y. Ding, J.M. Liu, J.L. Sun, W. Wang, Q.Y. Zheng, Highly crystalline covalent organic frameworks from flexible building blocks, Chem. Commun. 52 (2016) 4706–4709, https://doi.org/10.1039/c6cc01171c.

[51] M.J. Liu, J.N. Liu, K. Zhou, J.W. Chen, Q. Sun, Z.B. Bao, Q.W. Yang, Y.W. Yang, Q.L. Ren, Z.G. Zhang, Turn-on photocatalysis: Creating lone-pair donor-acceptor bonds in organic photosensitizer to enhance intersystem crossing, Adv. Sci. 8 (2021), 2100631, https://doi.org/10.1002/advs.202100631.

[52] W. Huang, J. Byun, I. Rorich, C. Ramanan, P.W.M. Blom, H. Lu, D. Wang, L.C. da Silva, R. Li, L. Wang, K. Landfester, K.A.I. Zhang, Asymmetric covalent triazine framework for enhanced visible-light photoredox catalysis via energy transfer cascade, Angew. Chem. Int. Ed. 57 (2018) 8316–8320, https://doi.org/10.1002/anie.201801112.

[53] L. Chen, L. Wang, Y.Y. Wan, Y. Zhang, Z.M. Qi, X.J. Wu, H.X. Xu, Acetylene and diacetylene functionalized covalent triazine frameworks as metal-free photocatalysts for hydrogen peroxide production: A new two-electron water oxidation pathway, Adv. Mater. 32 (2020), 1904433, https://doi.org/10.1002/adma.201904433.

[54] F. Haase, B.V. Lotsch, Solving the COF trilemma: Towards crystalline, stable and functional covalent organic frameworks, Chem. Soc. Rev. 49 (2020) 8469–8500, https://doi.org/10.1039/d0cs01027h.

[55] S.C. Wei, F. Zhang, W.B. Zhang, P.R. Qiang, K.J. Yu, X.B. Fu, D.Q. Wu, S. Bi, F. Zhang, Semiconducting 2D triazine-cored covalent organic frameworks with unsubstituted olefin linkages, J. Am. Chem. Soc. 141 (2019) 14272–14279, https://doi.org/10.1021/jacs.9b06219.

[56] R.H. Xu, W.R. Cui, C.R. Zhang, X.R. Chen, W. Jiang, R.P. Liang, J.D. Qiu, Vinylene-linked covalent organic frameworks with enhanced uranium adsorption through three synergistic mechanisms, Chem. Eng. J. 419 (2021) 129550, https://doi.org/10.1016/j.cej.2021.129550.

[57] Y. Kuwahara, T. Ando, H. Kango, H. Yamashita, Palladium nanoparticles encapsulated in hollow titanosilicate spheres as an ideal nanoreactor for one-pot oxidation, Chem. Eur. J. 23 (2017) 380–389, https://doi.org/10.1002/chem.201604081.

[58] Y. Kuwahara, R. Matsumura, H. Yamashita, Hollow titanosilicate nanospheres encapsulating PdAu alloy nanoparticles as reusable high-performance catalysts for a H₂O₂-mediated one-pot oxidation reaction, J. Mater. Chem. A 7 (2019) 7221–7231, https://doi.org/10.1039/c9ta01481k.